NASA Technical Memorandum 83771

Effect of Combined Pressure and Temperature Distortion Orientation on High-Bypass-Ratio Turbofan Engine Stability

Ronald H. Soeder and Charles M. Mehalic
Lewis Research Center
Cleveland, Ohio

October 1984

NASA

EFFECT OF COMBINED PRESSURE AND TEMPERATURE DISTORTION ORIENTATION ON HIGH-BYPASS-RATIO TURBOFAN ENGINE STABILITY

Ronald H. Soeder and Charles M. Mehalic
National Aeronautics and Space Administration
Lewis Research Center
Cleveland, Ohio 44135

SUMMARY

The effects of steady-state and quasi-steady-state combined 180°-extent circumferential-pressure and temperature distortions on inlet flow and internal engine performance were determined for a high-bypass-ratio turbofan engine. To measure performance at the engine inlet, the flow-angle, static-pressure, total-pressure, and total-temperature instrumentation was placed between the hydrogen burner or the rotatable-screen distortion-generator assembly and the engine inlet. Fan and compressor performance was measured using static-pressure, total-pressure, and total-temperature measurements located at the fan exit and compressor inlet and exit. In addition, static-pressure measurements were made in the passage upstream of the compressor face and at each stator stage inside the compressor.

Three 180°-extent circumferential screens were separately mounted on the rotatable assembly to provide different total-pressure distortion intensities and orientations. A hydrogen burner, capable of ±30° rotation from top dead center, produced various total-temperature distortion intensities and orientations. The mechanical fan speed at standard sea level conditions was rated at 7005 rpm. All experiments were conducted with a fan speed (corrected to the undistorted temperature sectors at station 1) of 90 percent of rated condition and a Reynolds number index of 0.5.

Free-stream yaw angle increased between the screen assembly and the engine inlet. The largest yaw angle variation occurred at the hub region of the engine inlet. The largest variation in both free-stream and tip boundary layer yaw angle occurred when combined pressure and temperature distortion was 180° out-of-phase.

Static-pressure distortion generated along the inlet duct wall by the screen assembly increased exponentially as flow approached the engine inlet. The static-pressure profile was flat at the compressor exit. Total-pressure and total-temperature profiles remained constant along the inlet duct. At the compressor exit the total-pressure profile was flat, and the total-temperature profile was sinusoidal for all combined distortion orientations investigated. The highest level of temperature distortion inside the compression system occurred when the combined 180°-extent distortions were overlapped at the engine inlet. The level of static-pressure distortion remained constant through the first five stages of the compressor and then decreased through the remaining stages.

The relationship between the level of total-pressure and total-temperature distortion which results in engine stall evolved into a engine stability map for the compressor inlet. The map shows a corridor of stable engine operation. The maximum total-pressure distortion at station 2C is 16.4

percent. The maximum total-temperature distortion at station 2C resulting in compressor stall is 33 percent.

INTRODUCTION

Future improvement in airbreathing propulsion engines is based on the ability to accurately predict the effects of nonuniform inlet flow on engine stability. These flow variations are discernible at the engine inlet in the form of pressure, temperature, or combined distortions. Analytical effort has recently resulted in the development of compressor models that predict the effects of inlet distortion on a turbojet engine (ref. 1) and on low-bypass-ratio turbofan engine performance (refs. 2 to 5). To evaluate these models, it is important to correctly define the actual flow fields entering and passing through the compression system in the presence of pressure, temperature, and combined pressure-temperature distortions. Low-bypass-ratio turbofan engine investigations dealing with temperature distortions are reported in references 6 to 9, and the effects of pressure distortion are presented in references 10 to 13.

This investigation was conducted to evaluate engine and compressor flow characteristics produced by combined 180°-extent pressure and temperature distortions of different intensities to provide a data base for evaluating high-bypass-ratio turbofan engine models. Evaluation of the combined inlet pressure-temperature distortions was achieved through the use of total pressure, static pressure, and total temperature probes installed in a YTF34 turbofan engine at the engine inlet, fan exit, and the compressor inlet and exit. Free-stream yaw flow angles were measured using flow-angle rakes at two axial stations between the distortion devices (hydrogen burner and rotatable screen assembly) and fan inlet. Static pressure taps were installed along the inlet-duct wall at two circumferential positions. Static-pressure variation upstream of an engine inlet is discussed in reference 14. Static pressure measurements were also made at each of the 13 stages inside the axial-flow compressor. The measurements were made at two circumferential locations for each stage.

Data are presented for a fan corrected speed of 90 percent of rated condition and a Reynolds number index of 0.5 (based on the undistorted sectors at station 1, the inlet flow measurement station). The pressure and temperature distortion extent was 180°. The screens used in the investigation produced pressure distortion levels up to 16.4 percent. The hydrogen burner was adjusted to produce temperature distortion levels between 6.7 and 33 percent. The above noted percent distortion levels occurred when combined distortion was present at the compressor inlet.

SYMBOLS

e	natural logarithm base
NFR2	fan speed corrected to station 2 test conditions, $NF/\sqrt{\theta_2}$, rpm
P	pressure, P_a
PNFR2	fan speed corrected to station 2 test conditions as percent of 7005 rpm

RNI	Reynolds number index, $\delta/(\mu/\mu_{sls})\sqrt{\theta}$
r_m	mean radius of inlet duct, 0.56 m
T	temperature, K
U	tangential velocity, m/sec
V	axial velocity, m/sec
x	axial length, m
β	yaw angle, deg
Δ	maximum-minimum value
δ	ratio of total pressure to standard sea level static pressure
θ	ratio of total temperature to standard sea level static temperature
μ	absolute viscosity, kg/(m-sec)

Subscripts:

s	static condition
sls	standard sea level static condition
T	total condition

Stations:

1	airflow metering station, located 126.64 cm upstream of engine inlet
1B	yaw measurement station behind distortion screen, located 57.62 cm upstream of engine inlet
1C	end of static pressure taps along inlet-duct wall, located 56.49 cm upstream of engine inlet
2	engine inlet-pressure, temperature, and flow angle measurement, located 14.96 cm upstream of engine inlet
2A	start of static pressure taps along inlet-duct wall, located 3.81 cm upstream of engine inlet
2C	compressor inlet; outer wall of passage located 57.91 cm downstream of engine inlet, inner wall of passage located 55.93 cm downstream of engine inlet.
2D	first-stage compressor stators
2E	second-stage compressor stators
2F	third-stage compressor stators
2G	fourth-stage compressor stators
2H	fifth-stage compressor stators
2I	sixth-stage compressor stators
2J	seventh-stage compressor stators
2K	eighth-stage compressor stators

2L	ninth-stage compressor stators
2M	tenth-stage compressor stators
2N	eleventh-stage compressor stators
2P	twelfth-stage compressor stators
2R	thirteenth-stage compressor stators
2.4	fan exit located 30.80 cm downstream of engine inlet
2.5	inlet to compressor flow passage; outer wall of passage is located 40.30 cm downstream of the engine inlet, inner wall of passage is located 37.25 cm downstream of engine inlet
2.6	compressor flow passage; outer wall of passage is located 46.88 cm downstream of engine inlet, inner wall of passage is located 43.42 cm downstream of engine inlet
2.7	compressor flow passage; outer wall of passage is located 51.53 cm downstream of engine inlet, inner wall of passage is located 49.72 cm downstream of engine inlet
3	compressor exit, located 121.23 cm downstream of engine inlet

APPARATUS

Engine

The engine used for this investigation was a YTF34 high-bypass-ratio (6.23 to 1) turbofan engine. A single-stage fan, with a rated pressure ratio of 1.51, was driven by a four-stage low-pressure turbine. The 14-stage axial-flow compressor had a nominal compression ratio of 14.5 and was driven by a 2-stage air-cooled high-pressure turbine. The engine was installed in an altitude chamber by a direct-connect type of installation (fig. 1). Engine schematic and instrumentation-station diagrams for the region upstream of the fan inlet and at the inlet, inter-stage, and exit of the compressor are presented in figure 2.

Distortion Devices

Inlet pressure distortion (pressure lower than average) was generated using one of three screen configurations with circumferential extents of 180° mounted on a rotatable screen assembly (fig. 3) located 0.692 m (27.24 in) upstream of the engine inlet. Distortion screen descriptions are given in table I.

A gaseous-hydrogen fueled burner was used to produce steady-state temperature distortions (temperature higher than average) at the engine inlet. The burner was installed in the plenum upstream of the inlet duct bellmouth (fig. 4). The burner had the capability of being rotated ±30° from the center position and was divided into four individually controlled quadrants. Air passing through the burner was heated in selected 90° sectors. Each 0° burner sector contained six swirl-can pilot burners to provide the ignition source

for the hydrogen. In addition, each 90° sector contained six annular gutters supported by one radial gutter and six circular-tube manifolds (one inside each annular gutter) with small holes for hydrogen injection. A hydrogen manifold located outside the burner was connected to the six circular tube-manifolds in each 90° sector by tubing and a flow control valve. The hydrogen manifold was connected to the hydrogen supply by additional lengths of tubing and a main flow control valve. The burner was located 3.81 m (150 in) upstream of the engine inlet.

Instrumentation

The instrumentation used to acquire the data is outlined in figures 2 and 5 to 7. Total and static pressures were recorded on scanivalves calibrated for a range of 103 to 1379 kPa (15 to 200 psia). These measurements included pressure levels at the flow metering location in the inlet duct (station 1), behind the distortion screen (stations 1B and 1C), and along the inlet duct, engine inlet, fan exit, and compressor inlet and exit.

Figure 6 shows the details associated with the yaw flow-angle pressure-measurement rake located at station 2. Yaw angle is positive when the tangential flow component is in the direction of fan rotation, as noted in figure 6. A flow-angle measurement was also made immediately behind the screen assembly at station 1B. Lastly, boundary layer yaw angle pressure probes were installed in the tip region at station 2 (see fig. 7). Flow angle probes were calibrated for a range of ±30° at the same free-stream Mach numbers encountered during engine experiments. The estimated error is ±1/2°. A more detailed description of flow-angle probes is found in reference 15.

Temperatures were measured from station 1 (flow measuring station) to the compressor exit (station 3) using chromel-alumel thermocouples, except at station 2.4 (fan duct) where copper-constantan thermocouples were used. Both types of thermocouples were referenced to a 339 K (610 °R) oven. Mach number recovery corrections used for thermocouples are discussed in reference 16.

PROCEDURE

Steady-state combined pressure and temperature distortions at the engine inlet were generated by a rotatable screen assembly (fig. 3) and a hydrogen burner (fig. 4). For the steady-state combined distortion investigation, the burner was set at the 0 or ±30° position. The screen was rotated in 90° increments between 0 and 360°. All angular positions noted are clockwise as viewed looking upstream from the aft end of the engine.

The first distortion orientation was with a 180° extent, 49.4 percent blockage screen (10 percent total-pressure distortion at the engine inlet) positioned from 0 to 180°. The burner was positioned at 0 (sector partitions are vertical and horizontal) and quadrants III and IV (see fig. 4) were ignited. The gaseous-hydrogen flow was then increased until the average temperature at the engine face from 180° to 360° was approximately 319 K (575 °R). The temperature from 0 to 180° was 289 K (520 °R). The temperature difference between heated and unheated quadrants produced a total-temperature distortion level of 10 percent at the engine inlet. When conditions at the engine inlet were stable, a data point was recorded. Quadrant III of the

burner was then shutdown, and the rotatable screen assembly was rotated 90° clockwise so that the screen extended from 90° to 270°. Quadrant I of the burner was then ignited, and hydrogen flow increased until quadrants I and IV produced a temperature level of approximately 319 K (575 °R) at the engine inlet (270° to 90° position). This procedure was continued until the 180°-extent pressure and temperature distortion was rotated over the entire engine face. Four steady-state data points were recorded at each burner angular position of -30°, 0, and +30°. The result is 12 data points per rake for each profile discussed in this investigation. The rotatable screen assembly and burner were positioned such that one of the following four configurations pertained: (1) the screen was 180° out-of-phase with the 180°-extent temperature distortion (previously discussed), (2) the screen preceded the 180°-extent temperature distortion by 90°, (3) the screen completely overlapped the 180° temperature distortion, and (4) the screen lagged the 180°-extent temperature distortion by 90°.

The next segment of this investigation entailed a compressor stability study. For the first experiment the heated sectors of the burner extended from 180° to 360°. The 180°-extent pressure distortion was positioned from 0 to 180°. The temperature distortion was increased at a constant rise rate low enough to provide quasi-steady-state conditions, until stall occurred. The pressure and temperature distortion orientation for this experiment was defined as being 180° out-of-phase. Similar compressor stability experiments included the following pressure and temperature distortion orientations: (1) temperature distortion from 0 to 180° and pressure distortion from 180° to 360°, and (2) pressure and temperature distortion overlap from (a) 0 to 180° or (b) from 180° to 360°. This process was repeated for two other distortion screens.

For combined pressure and temperature distortion tests, the presentation of a set of 12 data points for a pressure or temperature profile is as follows. The burner was set at 0, and the first data point was plotted at its installed angular rake (or tap) position. The second data point was then plotted at a step of 30°, but in the opposite direction to the rotation of the ignited burner sectors. This procedure is similar to holding the burner in a fixed position and rotating the instrumentation. Pressure and temperature data were normalized to upstream plenum pressures and temperatures in order to compensate for small run-to-run variations.

At each of the inlet duct wall static taps (fig. 5) at two circumferential locations, a maximum and minimum static pressure were identified for each test series of 12 data points. The difference between the maximum and minimum was normalized with a similar difference at the static taps nearest the engine inlet (station 2A, fig. 5) and presented as a relative static-pressure distortion level.

A constant Reynolds number index (RNI) of 0.5 was achieved by maintaining approximately a 289 K (520 °R) total temperature in the undistorted sectors of the burner and adjusting the engine inlet total pressure to obtain a value of 0.5 RNI at station 1. The fan mechanical speed was adjusted during steady-state combined distortion tests and at the start of the compressor stability experiments in order that the corrected fan speed based on the undistorted burner sectors was 90 percent of rated condition.

RESULTS

The effects of combined pressure and temperature distortion on inlet flow profiles were investigated. The influence of combined distortion orientation on inlet flow angle, inlet duct static-pressure distortion, fan inlet, compressor inlet, and compressor internal and exit pressure and temperature profiles are presented. The effect of combined distortion overlap on engine inlet stability are discussed. The 180°-extent pressure distortion varied from 6.8 to 16.4 percent, and the 180°-extent temperature distortion varied from 6.7 to 33 percent. These distortion levels occurred when combined distortion was present at the compressor inlet. The Reynolds number index at station 1 in the undistorted temperature sectors was set at 0.5, and the corrected fan speed was 90 percent of rated condition.

Flow Angle

Clean inlet. - The undistorted streamline yaw flow angles at station 1B are shown in figure 8. The yaw angle varied from -1.7° at the hub region to -2.5° at the midspan region. The free-stream yaw angle at station 2 varied from -0.1° at the hub to -2.7° at the tip region as shown in figure 9(a). The above noted yaw angle variations occurred at a corrected fan speed of 90 percent. A similar free-stream undistorted yaw flow angle compensation map at station 2 (engine inlet) was presented in reference 17. The tip boundary layeryaw angle at station 2 remained constant at +0.8° as shown in figure 9(b).

180° distortion. - Flow-angle data obtained at stations 1B and 2 when the fan speed was 90 percent of rated condition and RNI equal to 0.5 are presented in figures 10 to 12. The yaw angle variation with relative circumferential position immediately behind the rotatable screen assembly at station 1B, located 57.62 cm (22.69 in) upstream of the engine inlet, shows a profile that varies slightly within a data band of ±2.5° (see fig. 10). The nearly constant yaw angle profiles at station 1B is the result of an absence of the mixing of the two parts of the flow (no engine pumping effects). The orientation of the combined pressure and temperature distortions had no effect on hub and midspan yaw angle variation at station 1B.

Flow angle data presented in figures 11 and 12 were obtained with 180°-extent pressure and temperature distortion at station 2. The magnitude of each distortion was approximately 10 percent. Total-pressure and total-temperature distortions at station 2 are defined as

$$\frac{\left(P_{T,max} - P_{T,min}\right)}{P_{T,av}} \tag{1}$$

and

$$\frac{\left(T_{T,max} - T_{T,min}\right)}{T_{T,av}} \tag{2}$$

The maximum and minimum values in equation (2) refer to the maximum or minimum values of the rake average. The average pressure or temperature term refers to a face average value. The total-pressure distortion alues for all

screens tested at steady-state conditions with 0.5 RNI and 90 percent fan speed are listed in table I.

Free stream yaw angle variations at station 2 are presented in figure 11. The amplitude of the yaw angle variations increased as the flow approached the engine inlet for all four distortion orientations investigated. The largest variation occurs in the hub region for the orientation where pressure and temperature distortion are 180° out-of-phase (fig. 11(b)). For this configuration the range of the hub yaw angle is from +31° to -22.5°, which is several degrees larger, on an overall yaw angle variation basis, than the other three combined-distortion orientations investigated. An examination of the station 2 tip boundary layer profiles in figure 12 shows the largest variation also occurs for the orientation where pressure and temperature distortions are 180° out-of-phase. This result is similar to data presented in reference 8.

Consider the hub yaw angle profiles associated with pressure, temperature, or combined pressure and temperature distortion that are presented in figure 13. The slope of the yaw angle profile decreases for pressure distortion only and increases for temperature distortion only. The combined-distortion yaw angle profile where the 180°-extent pressure and temperature distortion are 180° out-of-phase with each other is similar to the profile associated with pressure distortion only. The profiles show that temperature distortion has only a weak effect on flow angle when compared with pressure distortion.

Static Pressure Distortion

The change of static-pressure distortion along the inlet duct wall from behind the rotatable screen assembly to the engine inlet is presented in figure 14. Data were recorded for 180°-extent pressure and temperature distortions at the engine inlet for four different combined distortion orientations. The static-pressure distortion change developed in reference 14 and presented in references 8 and 13 for a low-bypass-ratio turbofan engine and reference 17 for a high-bypass-ratio turbofan engine was found to hold for this investigation. The distortion change is defined as $(P_{s,max} - P_{s,min})$ for each location, normalized by $(P_{s,max} - P_{s,min})$ at station 2A or $(\Delta P_s)/(\Delta P_s)_{2A}$.

The data presented in figure 14 show that the relative static-pressure distortion does follow the exponential curve, as discussed in reference 14. The data in figure 14 diverge from the exponential curve for normalized distance parameter x/r_m values less than 0.26 and greater than 0.83. The axial location for station 2 rakes is at x/r_m = to 0.26, and the free-stream yaw angle rake located at station 1B is at $x/r_m = 1.03$. The aforementioned rakes produced a disruptive effect on air flow due to rake blockage of the inlet duct. In addition, the conical spinner mounted on the front of the engine causes an area change to occur before the streamlines enter the fan inlet. The theoretical curve presented in figure 14 holds for a constant area duct and can be mathematically expressed as

$$\frac{\Delta P_s}{(\Delta P_s)_{2A}} = e^{-[(x-x_{2A})/r_m]} \qquad (3)$$

The area change and rake blockage noted above all contributed to the divergence between the experimental data and the theoretical curve at stations 1B, 2, and 2A.

Pressure and Temperature Profiles at Inlet

Axial variation of total- and static-pressure and total-temperature profiles along inlet duct. - Figure 15 describes the axial variation of free-stream rake-average total pressures between station 1B (immediately behind the rotatable screen assembly) and station 2 (engine inlet). Also shown is the axial variation of free-stream rake-average total temperature between station 1 (downstream of the hydrogen burner) and station 2. The variation of inlet duct static-pressure profiles between station 1C (see fig. 5) and station 2 is also presented. The total-pressure and total-temperature profiles show little change in amplitude along the inlet duct as the flow approaches the engine inlet. The data show the relationship between the total-pressure and total-temperature profiles based on the orientation of two distortions (pressure and temperature). When the two distortions are 180° out-of-phase with each other, each half of the engine inlet (station 2) is subjected to only one type of distortion (see fig. 15(a)). Figure 15(b) shows these profiles when the pressure distortion precedes the temperature distortion by 90°. The total-pressure and total-temperature profiles of figure 15(c) occur when the 180°-extent distortion patterns are superimposed (180° overlapped) on each other and, therefore, half of the engine inlet is subjected to both distortions. The last combined distortion orientation occurs when the pressure distortion lags the temperature distortion by 90° (fig. 15(d)). The total-pressure and total-temperature profiles shown in figure 15(b) and 15(d) are identified as 90° overlapping combined distortions.

The static-pressure profiles of figures 15(a) to (d) show that the amplitude of the sinusoidal profiles increases between station 1C (nearest to the screen) and station 2 for each of the four combined distortion orientations investigated. The increase in static-pressure profile amplitude along the inlet duct was also shown in figure 14. The largest amplitude variation in static-pressure profiles occurs in the hub region at station 2.

The hub static-pressure profiles at station 2 are shown in figure 16. An examination of the profiles between 0 to 180° shows that the lowest static-pressure level occurs when the distortion is produced entirely by a screen. Over the 0 to 90° sector, pure pressure distortion occurs when (1) pressure and temperature distortion are 180° out-of-phase with each other and (2) pressure distortion precedes temperature distortion by 90°. Similarly, pure pressure distortion occurs over the 90° to 180° sector when (1) pressure distortion and temperature distortion are 180° out-of-phase and (2) temperature distortion precedes pressure distortion by 90°. The data below 1.0 from 0 to 180° in figure 16 verify that the streamlines are entering a low-pressure region.

Compression System Pressure and Temperature Profiles

Pressure and temperature profiles at fan exit. - Normalized total-pressure, total-temperature, and static-pressure profiles at the fan exit (station 2.4) are shown in figure 17. The total-pressure and total-

temperature profiles at station 2.4 have a sinusoidal shape. (Those at the inlet (station 2) have square wave profiles at the engine inlet (fig. 15)). The transition from square to sinusoidal shape indicates the circumferential blending that occurred in the fan.

An examination of the total-pressure profiles at station 2.4 (see figs. 17(a-1) to 17(d-1)) shows that a shift of 7.5° to 30° in the direction opposite to fan rotation occurs in the low pressure region of the profiles (data below 1.0), depending on the combined distortion orientation at station 2. This rotation of the profiles can be attributed to the redirection of the flow by the fan exit guide vanes.

If we compare the circumferential extents of the total-temperature profiles at station 2.4 that are above 1.0 (temperature distorted region) with the circumferential extents of the profiles at station 2 that are above 1.0, a shift in the profiles in the direction of fan rotation occurs at station 2.4. This is observed in comparing figures 17(b-2), (c-2), and (d-2) with figures 15(b-2), (c-2), and (d-2). The station 2.4 profiles have rotated from a minimum of 16.5° (figs. 17(b-2) and (d-2)) to a maximum of 22.5° (fig. 17(c-2)) in the direction of fan rotation. The temperature profile rotation is the result of temperature passing through a fan or compressor along a particle path (a property of state) as compared with pressure, which passes through rotating components as a wave (ref. 3). The amplitude of the temperature profiles at station 2.4 is due to the temperature distortion that exists at station 2 plus the increased temperature rise that occurs in the fan due to pressure distortion.

Static-pressure profiles upstream of compressor inlet. - The static-pressure profiles at station 2.5 in the compressor flow passage between the fan exit and compressor inlet are shown in figure 18. The profiles have a sinusoidal configuration for each of the four combined distortion orientations investigated, and there is no difference in profile amplitude between hub and tip statics located in the passage. A comparison of the static-pressure profiles at station 2.5 (fig. 18) and station 2.4 (fan exit; see fig. 19) shows an increase in profile amplitude resulted from compressor pumping effects and to a lesser extent the reduction in flow passage area from the fan exit to the compressor flow passage upstream of the compressor inlet. Another comparison of the sinusoidal static-pressure profiles at station 2.5 (see fig. 18) with the profiles at the engine inlet (station 2; see fig. 16) shows that the low pressure region at station 2 (data below 1.0) is from 0 to 180° and that at station 2.5 the low pressure region is from 330° to 150°. This indicates that a 30° rotation of the static-pressure profile in the direction opposite to that of fan rotation has occurred. This shift is similar to that discussed previously for the total-pressure profiles at station 2.4.

Static-pressure profiles at stations 2.6 and 2.7 along the compressor flow passage upstream of the compressor inlet are shown in figure 19. The data presented are for combined distortion orientations where pressure and temperature distortion are 180° out-of-phase. Similar profiles were obtained for the other three distortion orientations investigated and are not shown. The static-pressure profiles at stations 2.6 and 2.7 have a sinusoidal configuration, and the hub and tip data are coincident. The amplitude and 30° profile shift present at the fan exit also exists at stations 2.6 and 2.7.

Pressure and temperature profiles at compressor inlet. - Normalized total-pressure, total-temperature, and static-pressure profiles at the compressor inlet (station 2C) are shown in figure 20. The total-pressure profiles (see figs. 20(a-1) to (d-1)) show that 180°-extent pressure distortion occurred at the compressor face regardless of the distortion orientation. The total-pressure distortion extent between the engine inlet and compressor inlet was therefore maintained. The shape of the total-pressure profiles changed from a square wave form at station 2 (engine inlet) to a double exponential wave form (an increasing exponential curve followed by a decreasing exponential curve after a peak value is attained) at the compressor inlet.

The total-temperature profiles have a sinusoidal configuration and the distortion extents varied from 165°, where combined distortions are 180° out-of-phase (fig. 20(a-2)) and pressure distortion precedes temperature distortion by 90° (fig. 20(b-2)), to 174°, where temperature distortion precedes pressure distortion by 90° (fig. 20(d-2)). This represents a small reduction in 180°-extent temperature distortion which occurs at the fan exit (see fig. 17). In addition the temperature profiles at station 2C have rotated further in the direction of fan rotation from their circumferential positions at station 2.4. The rotation varied from 22.5° when pressure distortion precedes temperature distortion by 90° (see fig 20(b-2)) to 30° when pressure and temperature distortion are 180° out-of-phase (fig. 20(a-2)) and pressure and temperature distortion overlap (fig. 20(c-2)). This rotation of the temperature profiles was previously discussed in conjunction with figure 17.

The static-pressure profiles at station 2C have a sinusoidal configuration (figs. 20(a-3) to 20(d-3)). The hub static data are at a lower level than the tip static data over the pressure distorted extent, indicating a larger distortion amplitude in the hub region of the compressor inlet. The hub and tip static relationship at the compressor face was similar for all the combined distortion orientations investigated.

Static-pressure profiles inside compressor. - Normalized face average static-pressure profiles from the first-stage stators (station 2D) to the 13th-stage stators (station 2R) are shown in figure 21. Only the odd-numbered stator stages inside the compressor are discussed, but similar results were obtained for the even-numbered compressor stator stages for the orientations investigated. Static-pressure profiles are shown when the combined distortions at the engine inlet were 180° out-of-phase or 180° overlapped (figs. 21(a) and (b)). The 90° combined distortion orientations are not shown as the profile amplitudes fell between the levels shown in figures 21(a) and 21(b).

Static-pressure variations which occur in the first and third compressor stator stages when 180° out-of-phase combined pressure and temperature distortion occurs at the engine inlet are presented in figure 21(a-1). It is observed that the profiles have a sinusoidal configuration and the amplitude remains constant between the first and third-stator stages. The extent of low pressure (data below 1.0) remains constant between the first and third-stage stators as the pressure distortion wave passes through the compressor. The static-pressure distortion over the first three stator stages is 10.5 percent. Examination of the profiles in figures 21(a-2) and (a-3) shows that the amplitude of the profiles continues to decrease through the compressor and approaches a flat profile in the 11th and 13th-stator stages, which indicates a low level of static-pressure distortion.

Superimposed (180° overlapped) pressure and temperature distortion at the engine inlet results in static-pressure variation in the firstand third-stator compressor stages, which is presented in figure 21(b-1). The profile amplitude between the first- and third-stator stages remains constant and is equal to 10.2 percent Examination of figure 21(b-2) shows that the profile amplitude at the fifth-stage stators is equivalent to the profile amplitude in the first and third-stage stators. The profile amplitudes at the seventh and ninth-stage stators are markedly reduced, and static-pressure distortion levels are 8.7 and 4.8 percent, respectively. The profile amplitudes in the 11th and 13th stages (fig. 21(b-3)) are further reduced and approached a flat profile, which indicates that the level of static-pressure distortion tends toward zero in the latter stages of the compressor. The reduction in profile amplitude for both distortion orientations presented in figure 21 shows the characteristic of the compressor to reduce the level of static-pressure distortion.

Pressure and temperature profiles at compressor exit. - Normalized total-pressure, total-temperature, and static-pressure profiles at the compressor exit (station 3) are shown in figure 22. The profiles are the result of 180° out-of-phase combined pressure and temperature distortion (see fig. 22(a)) or 180° overlapped combined pressure and temperature distortion (see fig. 22(b)) imposed at the engine inlet. The 90° combined distortion overlaps are not presented as the profile amplitudes fell within the levels presented in figures 22(a) and (b).

The total-pressure and static-pressure profiles for the 180° out-of-phase and 180° overlapped combined distortion orientations are flat. This demonstrates the characteristics of the compression system to reduce the total- and static-pressure distortion at the engine inlet from 10 percent to zero at the compressor exit.

The total-temperature profiles at station 3 which result from 180° out-of-phase and 180° overlapped combined engine inlet pressure and temperature distortion are presented in figures 22(a-2) and (b-2). The shape of the normalized total-temperature profiles at station 3 is sinusoidal, and the extent of the temperature profile that is above 1.0 is 174° in figure 22(a-2) and 165° in figure 22(b-2). Temperature data above 1.0 at the compressor exit indicates that temperature distortion has persisted through the engine compression system.

The station 3 temperature profile amplitude for 180° out-of-phase combined engine inlet pressure and temperature distortion (fig. 22(a-2)) is one-half the level of the profile at station 2 (engine inlet, fig. 15(a-2)). This is the result of the above average temperature rise associated with the greater pressure ratio in the pressure distorted sector of the engine. (A pure pressure distortion will generate a temperature distortion at the compressor exit.) Since the temperature distortion sector has less than the average pressure ratio, there is a decrease in temperature ratio; that is, the amount of temperature distortion will thus decrease.

The temperature profile at station 3 which results from 180° overlapped distortion at the engine inlet (fig. 22(b-2)) has an amplitude level which is approximately 2.3 percent larger than that at station 2. It would be expected that, in the case of the aligned distortions, the temperature distortion at the compressor exit would be greater than that at the engine inlet, in as much as the higher pressure ratio in the heated sector would result in higher temperature ratios.

The total-temperature profiles at station 3 have rotated in the direction of compressor rotation from their circumferential locations at station 2C. A comparison of figures 20(a-2) and 22(a-2) shows that the temperature profile rotated 173° for the 180° out-of-phase distortion. Similarly, a comparison of figures 20(c-2) and 22(b-2) shows that the temperature profile rotated 105° for the 180° overlapped distortion. The relative swirl angle between the pressure and temperature distortions for the 180° opposed distortions is larger than for the 180° overlapped distortions. This difference in relative swirl angle causes the temperature profile associated with opposed pressure and temperature distortion to rotate 68° more in the direction of compressor rotation then the temperature profile associated with overlapped combined distortions. A detailed description of flow swirl is presented in reference 3.

Variations in Compression-System Distortion

The amplification or attenuation of total-pressure, total-temperature, and static-pressure distortions are shown in figure 23. These distortion amplitudes were generated using maximum and minimum total-pressure and total-temperature rake averages or static-pressure tap values along with face-average conditions at each instrumented engine station. Maximum amplitudes are shown for opposed and overlapped 180°-extent combined pressure and temperature distortion orientations at station 2. The amplitudes associated with the 90° overlapped distortions are not shown since these maximum amplitudes fell within those presented in figure 23.

The total-pressure distortion increased for both configurations between the engine inlet and the compressor inlet (fig. 23(a)). Total-pressure distortion at the compressor inlet was 12.2 percent for overlapped distortions and 16.6 percent for opposed distortions. The total-pressure distortion at the compressor exit was equal to a range from 2.5 to 3.2 percent. The low level of distortion at the compressor exit (station 3) agrees with the flat total-pressure profiles presented in figures 22(a-1) and (b-1).

The total-temperature distortion amplitude profiles are shown in figures 23(b). The total-temperature distortion amplitude continues to increase through the compression system for the case of overlapped distortions. The level of temperature distortion at the compressor inlet and outlet is 12.9 and 13.8 percent, respectively. The level of temperature distortion amplitude for the case of opposed distortions at the engine inlet increased to 11.8 percent at the compressor inlet and decreased to 7.2 percent at the compressor exit.

Static-pressure distortion decreased between the engine inlet and fan exit when static-pressure measurements at the fan hub were used to calculate distortion amplitudes (see fig. 23(c)). The profiles then increased from the fan exit to station 2.7 (compressor flow passage upstream of the compressor inlet) due to compressor pumping effects. The static-pressure profile associated with overlapped combined distortion at the engine inlet remained a nearly constant 10 percent from station 2C through the fifth-stage stators (station 2H). The distortion level then decreased through the remainder of the compressor to a level of 2.6 percent at the compressor exit (station 3). The static-pressure profile associated with opposed distortion at the engine inlet shows similar results except the distortion level at the compressor inlet is 9.7 percent. The flat static-pressure profiles at station 3 (figs. 22(a-3) and (b-3)) verify the low-level of distortion at the compressor exit.

Stability Limits

The effects of various combinations of 180°-extent pressure and temperature distortions that resulted in compressor stall were experimentally determined. The rated mechanical fan speed at sea level conditions is 7005 rpm; this investigation was conducted with a fan speed (corrected to the undistorted sectors at station 1) of 90 percent of rated and a RNI of 0.5. References to the left or right side of the engine face are based on looking upstream from the aft end of the engine. In the calculation of total-pressure distortion amplitudes at station 2 the minimum and maximum total-pressure rake averages were used. Conversely, in the calculation of total-temperature distortion amplitudes at station 2, a maximum total-temperature rake average was used in the distorted sectors and a minimum total-temperature rake average was used in the undistorted sectors. The average total-pressure and total-temperature levels refer to face average conditions.

Opposed and superimposed distortions. - The effect of various intensities of opposed (no overlap) and superimposed (180° overlap) combined distortion on compressor stall are presented in figure 24. Data presented in the figure were obtained through the use of the three 180°-extent screens described in Table I. The amount of pressure distortion required to stall the engine compression system for various levels of temperature distortion is shown in the figure (shaded symbols), which is divided into four distinct regions. Region 1 represents the orientation where both temperature and pressure distortion are 180° out-of-phase. Region 4 represents the orientation where temperature and pressure distortion are superimposed. Region 2 is the spacial opposite of region 4. Region 3 is the spacial opposite of region 1.

The dashed lines in figure 24 represent estimated stall lines using simple parallel compressor theory. It should be noted that the compressor has variable inlet guide vanes followed by five variable-stator stages. In order to accurately predict compression system stall lines, off-design compressor-stage maps are required. These off-design maps were not available for this analysis.

The maximum temperature distortion in region 1 that resulted in compressor stall was approximately 33 percent. In region 3, the spacial opposite of region 1, the maximum temperature distortion was in the range of 18 percent. The difference in temperature distortion levels is attributed to a temperature sensor installed in the fan duct by the engine manufacturer. The sensor is located at the 270° position as viewed from the aft end of the engine. The sensor provides the engine fuel control with an airstream temperature signal which, in turn, adjusts the fuel control acceleration and deceleration schedules. Higher temperatures entering the fan and compressor inlet from 180° to 360° cause the sensor to send a signal to the fuel control which adjusts the acceleration and deceleration schedules to higher levels and permits engine operation at higher temperature levels before compressor stall occurs (region 1). Conversely, standard conditions of temperature entering the fan and compressor inlet from 180° to 360° cause the sensor to send a signal to the fuel control, which lowers the acceleration and deceleration schedules and results in lower temperature levels at which compressor stall occurs (region 3).

In the absence of a temperature sensor tied to the engine fuel control, the corridor of stall-free operation with temperature distortion extends from

±33 percent. The maximum pressure distortion required to stall the engine was not determined in these tests, but simple parallel compressor theory indicates that it would be 20 percent (y-axis intercept in fig. 24). A detailed discussion of the experimental effects of pressure and temperature distortion and analytical predictions based on a model for turbojet and turbofan engine performance is presented in reference 18. The compressor model of that reference shows that corrected speed is the critical temperature sensitive parameter.

SUMMARY OF RESULTS

A TF34 high-bypass-ratio turbofan was tested with combined 180°-extent inlet pressure and temperature distortions. The results of the experiments are as follows:

1. Yaw angle variation increased as airflow approached the engine inlet.

2. Yaw angle variation was largest in the hub region of the engine inlet when pressure and temperature distortions are 180° out-of-phase.

3. Tip boundary layer yaw angle variation at the fan inlet was largest when pressure and temperature distortions are 180° out-of-phase.

4. Static-pressure distortion increased exponentially between the distortion screen and the engine inlet paralleling the increase in flow angle.

5. Total-pressure circumferential profiles and total-temperature circumferential profiles remained constant along the inlet duct between the distortion devices (screen or burner) and the engine inlet.

6. Normalized total-pressure circumferential profiles varied from a square wave at the engine inlet to a flat profile at the compressor exit.

7. Normalized total-temperature circumferential profiles varied from a square wave at the engine inlet to a sinusoidal profile at the compressor exit.

8. Normalized static-pressure circumferential profiles varied from a sinusoidal profile at the engine inlet to a flat profile at the compressor exit.

9. The highest level of compressor exit temperature distortion occurred when combined 180°-extent pressure and temperature distortion overlapped (superimposed distortions) at the fan inlet.

10. For all combined inlet distortion orientations investigated, the level of static-pressure distortion inside the compressor remained a constant 10 percent through the first five stages. In the remainder of the compressor, the static-pressure distortion decreased to 3 percent.

11. An engine inlet stability map shows that the limiting total-pressure distortion based on simple parallel compressor theory is 20 percent. The range of total-temperature distortion is 18 to 33 percent (based on combined distortion orientation at the compressor inlet).

REFERENCES

1. Tesch, W.A.; and Steenken, W. G.: Blade Row Dynamic Digital Compression Program. Volume II - J85 Circumferential Distortion Redistribution Model, Effect of Stator Characteristics, and Stage Characteristics Sensitivity Study. (R76AEG484, General Electric Co.; NASA Contract NAS3-18526). NASA CR-134953, 1978.

2. Mazzawy, R. S.: Multiple Segment Parallel Compressor Model for Circumferential Flow Distortion. J. Eng. Power, vol. 99, no. 2, Apr. 1977, pp. 288-296.

3. Mazzawy, R. S.; and Banks, G. A.: Modeling and Analysis of the TF30-P-3 Compressor System with Inlet Pressure Distortion. (PWA-5302, Pratt & Whitney Aircraft; NASA Contract NAS3-18535). NASA CR-134996, 1976.

4. Mazzawy, R. S.; and Banks, G. A.: Circumferential Distortion Modeling of the TF30-P-3 Compression System. (PWA-5448, Pratt & Whitney Aircraft; NASA Contract NAS3-18535). NASA CR-135124, 1977.

5. Braithwaite, W. M.; and Soeder, Ronald H.: Combined Pressure and Temperature Distortion Effects on Internal Flow of a Turbofan Engine. AIAA Paper 79-1309, June 1979.

6. Braithwaite, Willis M.: Experimental Evaluation of a TF30-P-3 Turbofan Engine in an Altitude Facility: Effect of Steady-State Temperature Distortion. NASA TM X-2921, 1973.

7. Abdelwahab, Mahmood: Effects of Temperature Transients at Fan Inlet of a Turbofan Engine. NASA TP-1031, 1977.

8. Soeder, Ronald H.; and Bobula, George A.: Effect of Steady-State Temperature Distortion and Combined Distortion on Inlet Flow to a Turbofan Engine. NASA TM-79237, 1979.

9. Abdelwahab, Mahmood: Effects of Fan Inlet Temperature Disturbances on the Stability of a Turbofan Engine. NASA TM-82699, 1981.

10. Braithwaite, Willis M.; Dicus, John H.; and Moss, John E., Jr.: Evaluation of a Turbofan Engine of Air Jets as a Steady-State Inlet Flow Distortion Device. NASA TM X-1955, 1970.

11. Evans, David G.; et al.: Some Comparisons of the Flow Characteristics of a Turbofan Compressor System with and without Inlet Pressure Distortion. NASA TM X-71574, 1974.

12. de Bogdan, Claude E.; et al.: Effect of a 180° Extent Inlet Pressure Distortion on the Internal Flow Conditions of a TF30-P-3 Engine. NASA TM X-3267, 1975.

13. Soeder, Ronald H.; and Bobula, George A.: Effect of Steady-State Pressure Distortion on Flow Characteristics Entering a Turbofan Engine. NASA TM-79134, 1979.

14. Plourde, G. A.; and Stenning, A.H.: Attenuation of Circumferential Inlet Distortion in Multistage Axial Compressors. J. Aircr., vol. 5, no. 3, May-June 1968, pp. 236-242.

15. Dudzinski, T. J.; and Krause, L. N.: Flow-Direction Measurement with Fixed-Position Probes. NASA TM X-1904, 1969.

16. Glawe, George E.; Simmons, Frederick S.; and Stickney, Truman M.: Radiation and Recovery Corrections and Time Constarts of Several Chromel-Alumel Thermocouple Probes in High-Temperature, High-Velocity Gas Streams, NACA TN-3766, 1956.

17. Soeder, Ronald H.; and Bobula, George A.: Effect of Steady-State Pressure Distortion on Inlet Flow to a High-Bypass Ratio Turbofan Engine. NASA TM-82964, 1982.

18. Graber, Edwin J., Jr.; and Braithwaite, Willis M.: Summary of Recent Investigations of Inlet Flow Distortion Effect on Engine Stability. NASA TM X-71505, 1973.

TABLE I. - SCREEN DESCRIPTION

Screen	Wire diameter		Width of opening		Blockage,[a] percent	Total pressure distortion,[b] $(\Delta P_T/P_T)_2$ percent
	cm	in	cm	in		
1	0.081	0.032	0.201	0.079	49.4	10.0
2	.104	.041	.213	.084	54.8	12.7
3	.183	.072	.325	.128	59.0	14.3

[a]All screens were 180° in extent.

[b]$(P_{T,max} - P_{T,min}/P_{T,avg})$ at 90 percent fan speed, 0.5 RNI undistorted and no temperature distortion.

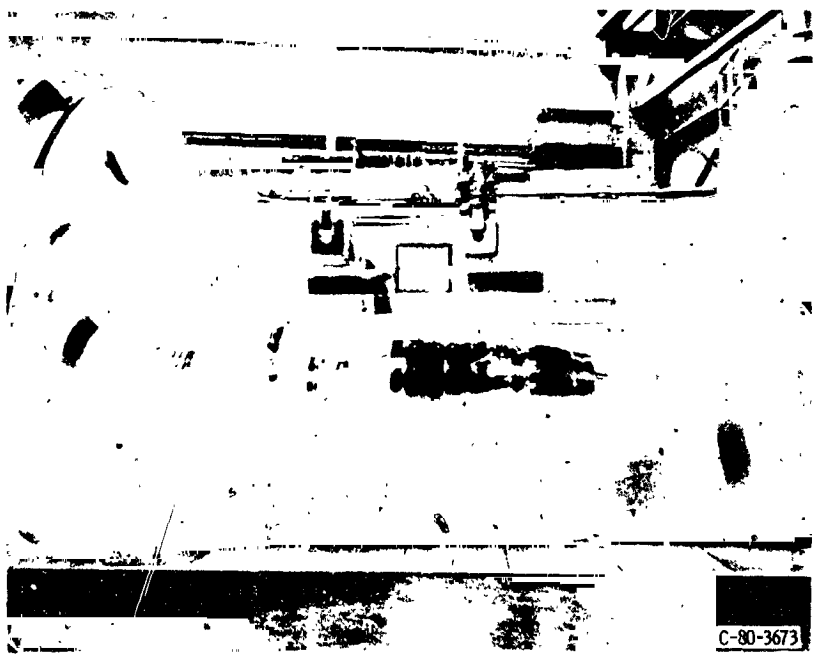

Figure 1. - TF34 engine in altitude test chamber.

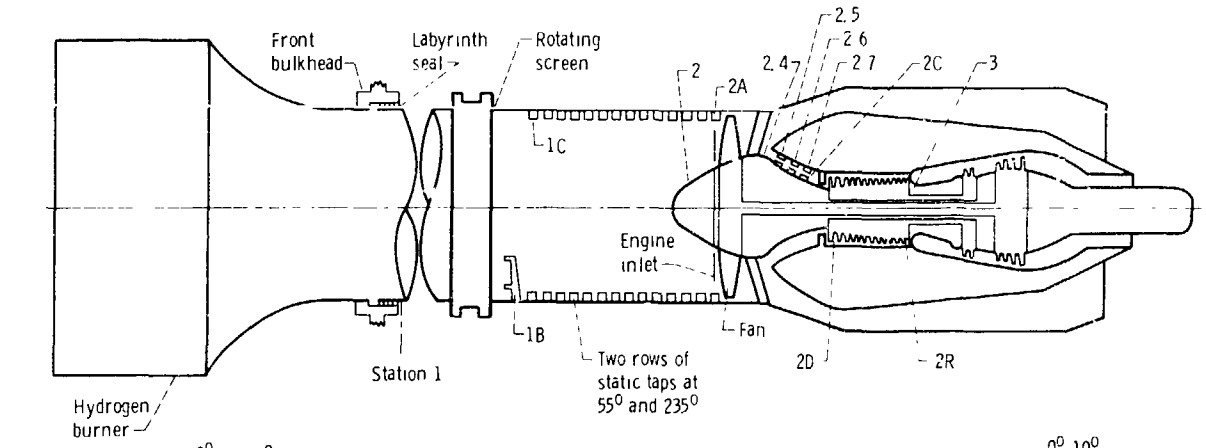

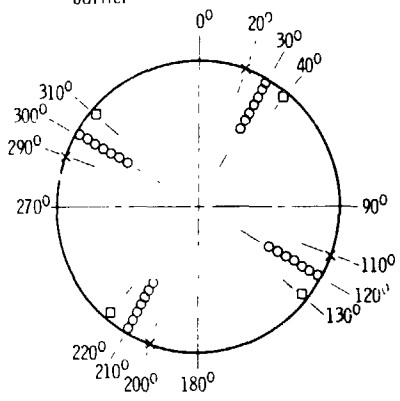

Station 1

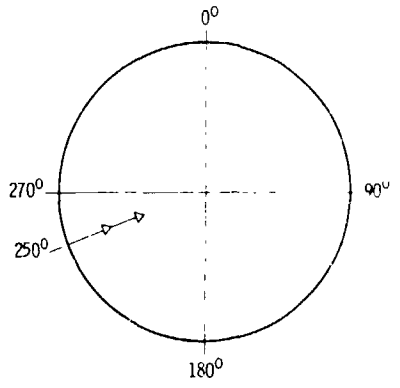

Station 1B

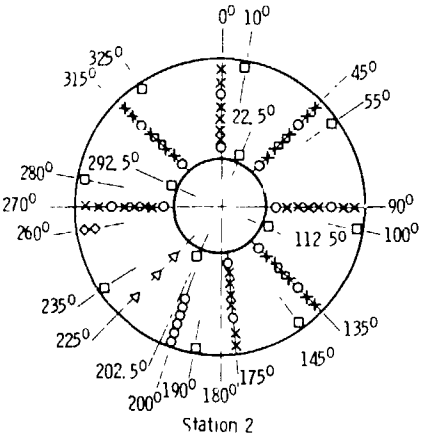

Station 2

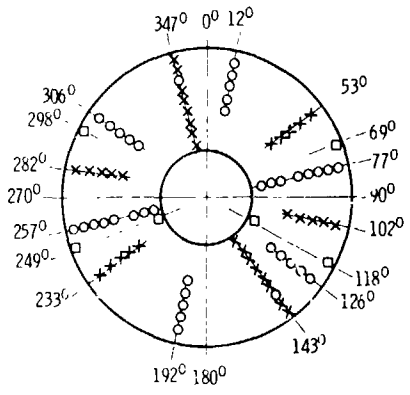

Station 2.4

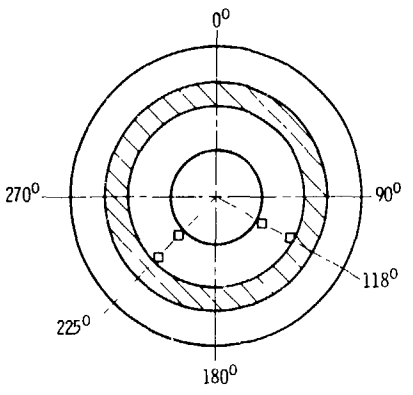

Stations 2.5, 2.6 and 2.7

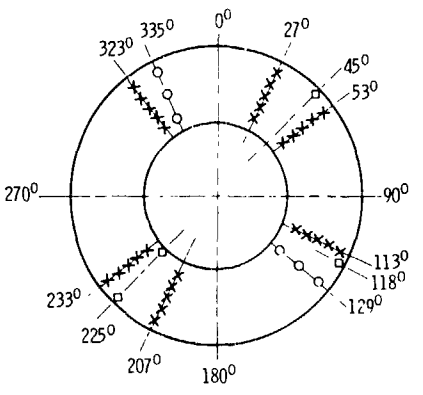

Station 2C

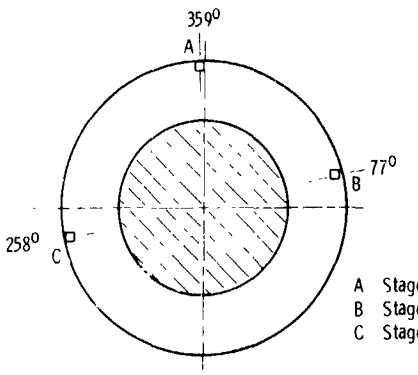

A Stages 1 to 5
B Stages 6 to 13
C Stages 1 to 13

Stations 2D to 2R

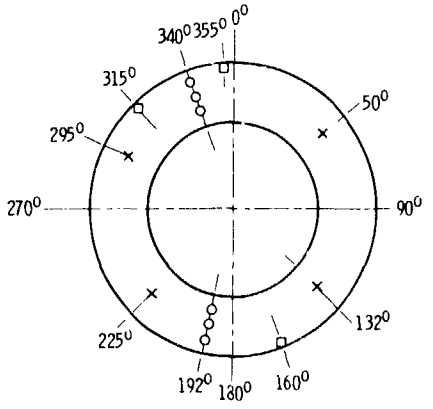

Station 3

- × Steady-state total temperature
- ○ Steady-state total pressure
- □ Steady-state static pressure
- △ Yaw pressure probe
- ◇ Boundary layer yaw probe

Figure 2. - Instrumentation layout for TF34 turbofan engine. (Stations viewed looking upstream. See symbols for description of station locations.)

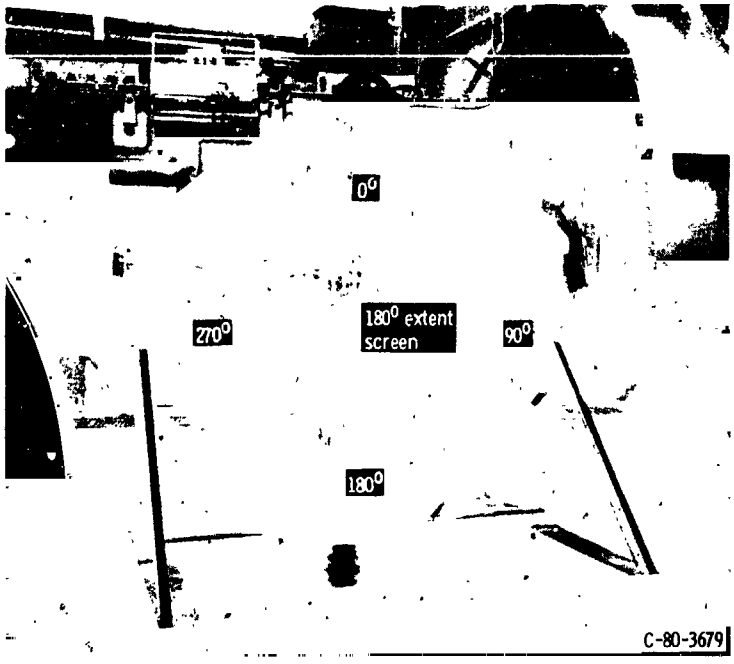

Figure 3. - Rotatable screen assembly, viewed from aft end of engine.

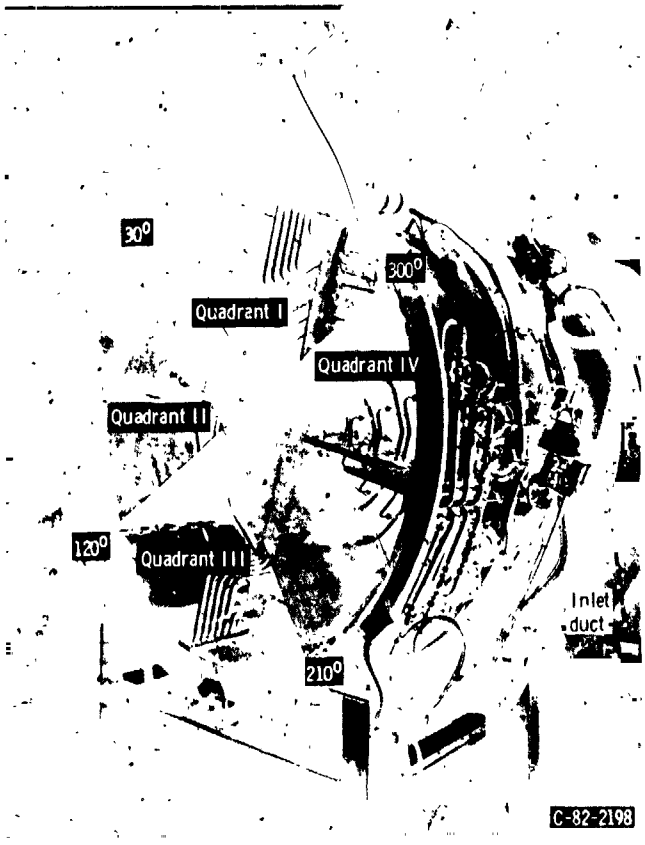

Figure 4. - Gaseous-hydrogen-fueled burner viewed in the direction of engine inlet.

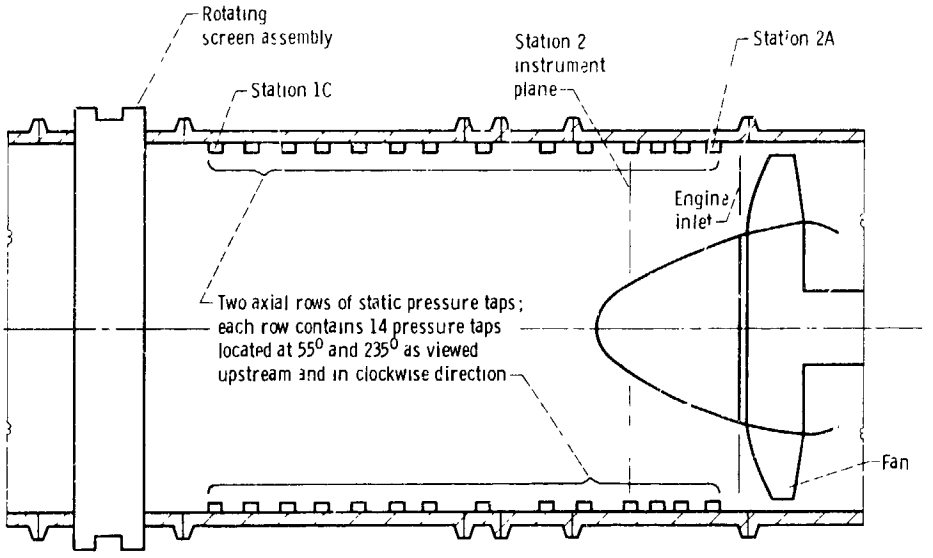

Figure 5. - Inlet ducting assembly.

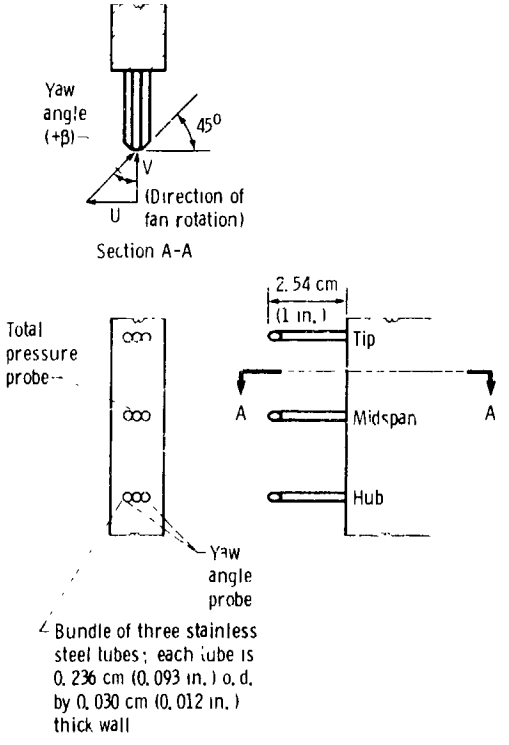

Figure 6. - Station 2 yaw-angle measurement rake.

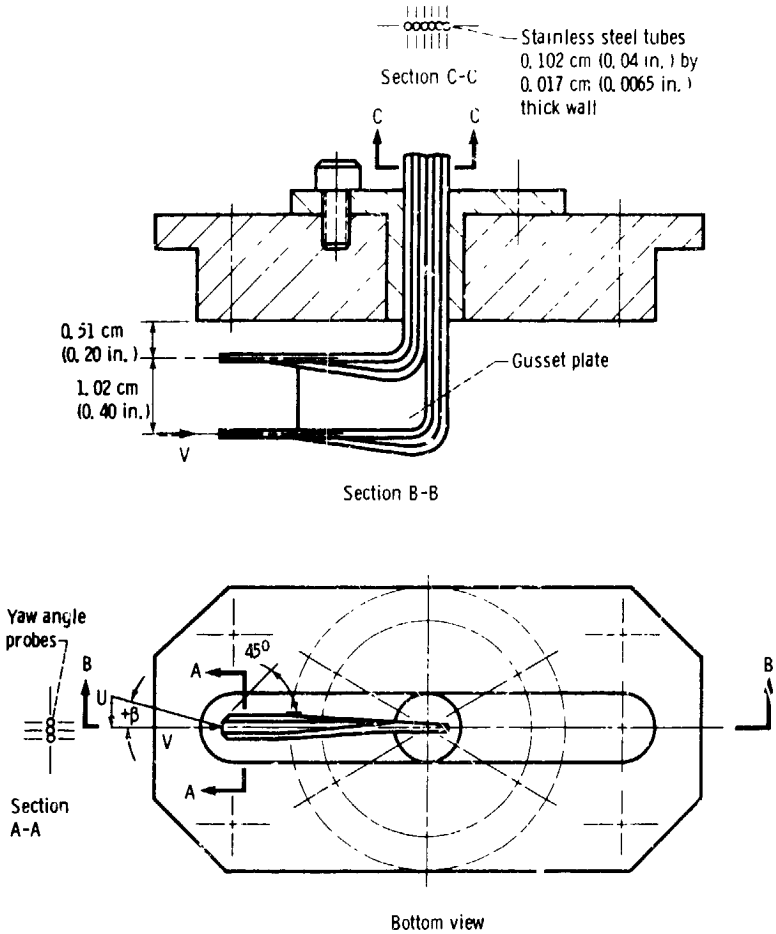

Figure 7. - Tip boundary layer yaw probes located at station 2.

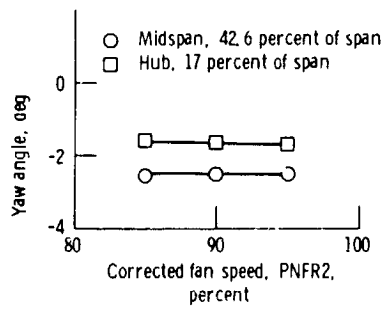

Figure 8. - Flow angle at station 1B versus corrected fan speed with no pressure or temperature distortion (clean inlet).

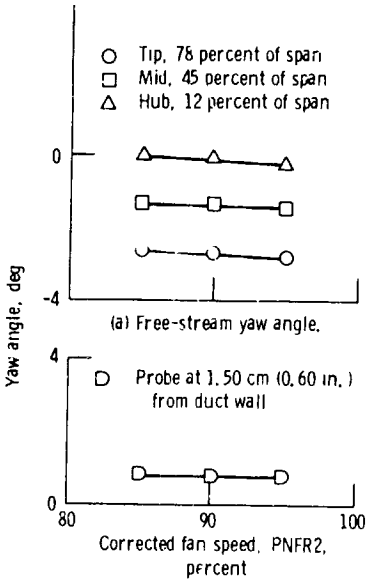

Figure 9. - Flow angle at station 2 versus corrected fan speed with no pressure and temperature distortion (clean inlet).

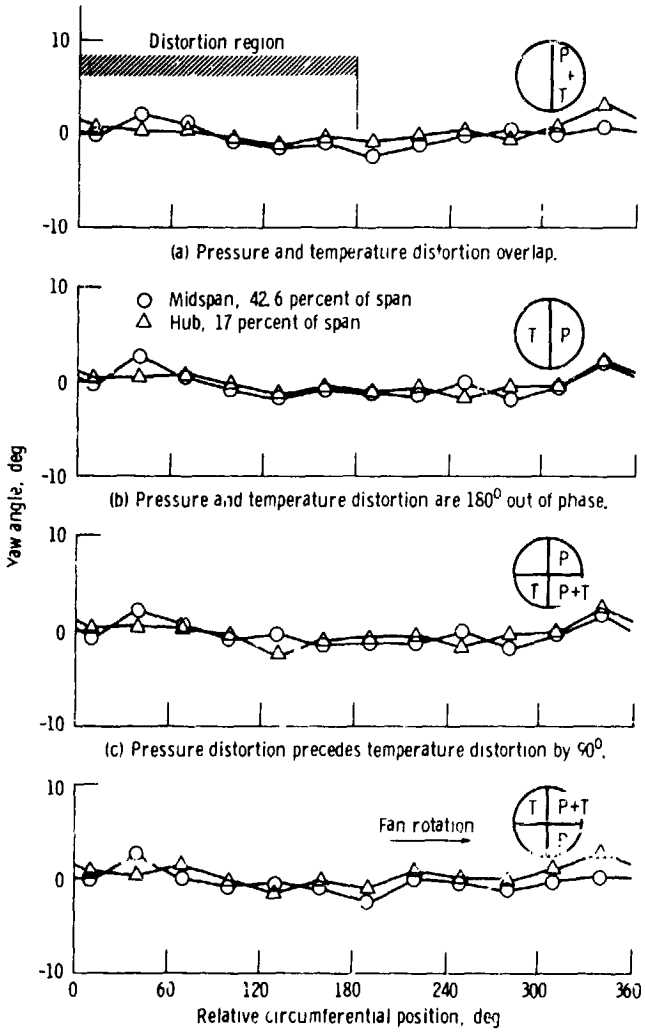

(a) Pressure and temperature distortion overlap.

(b) Pressure and temperature distortion are 180° out of phase.

(c) Pressure distortion precedes temperature distortion by 90°.

(d) Temperature distortion precedes pressure distortion by 90°.

Figure 10. - Yaw angle variation at station 1B with combined total-pressure and total-temperature distortion.

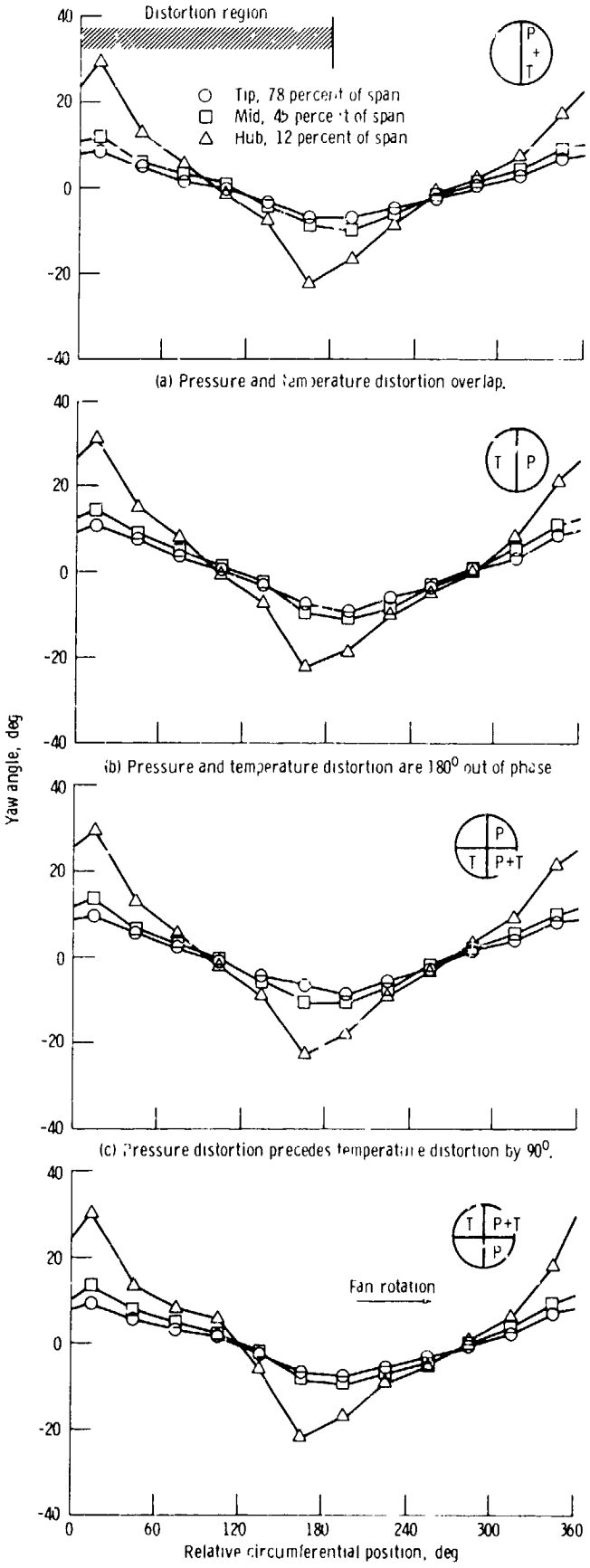

(a) Pressure and temperature distortion overlap.

(b) Pressure and temperature distortion are 180° out of phase

(c) Pressure distortion precedes temperature distortion by 90°.

(d) Temperature distortion precedes pressure distortion by 90°.

Figure 11. - Free-stream yaw angle variation at fan inlet (station 2) with combined total-pressure and total-temperature distortion

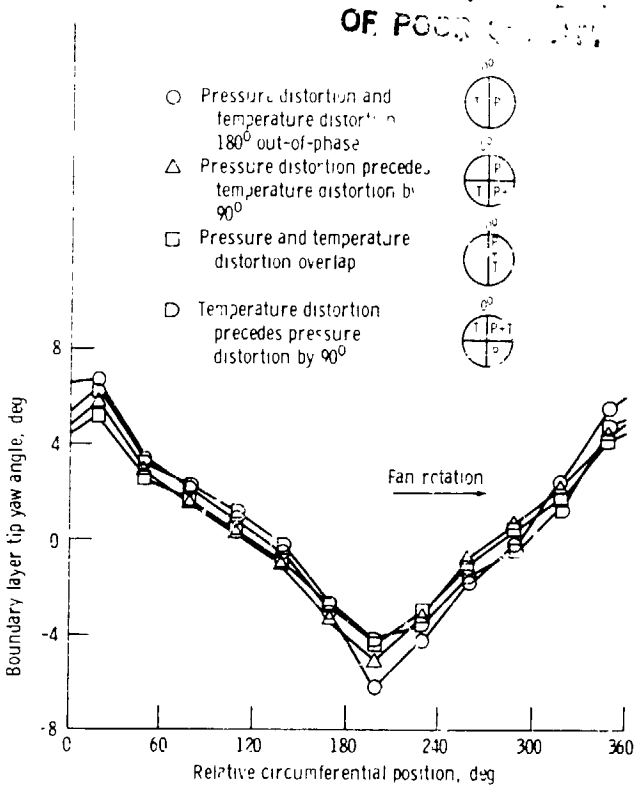

Figure 12 - Boundary layer tip yaw angle variation at station 2 for combined total-pressure and total-temperature distortion

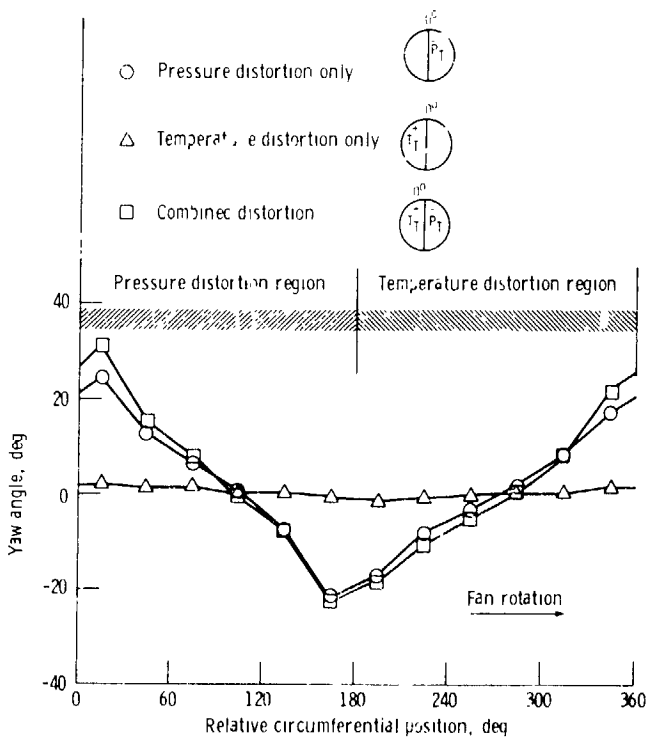

Figure 13. - Hub yaw angle variation at station 2 for 10 percent total-pressure, 9 percent total-temperature, and 10 percent combined distortions.

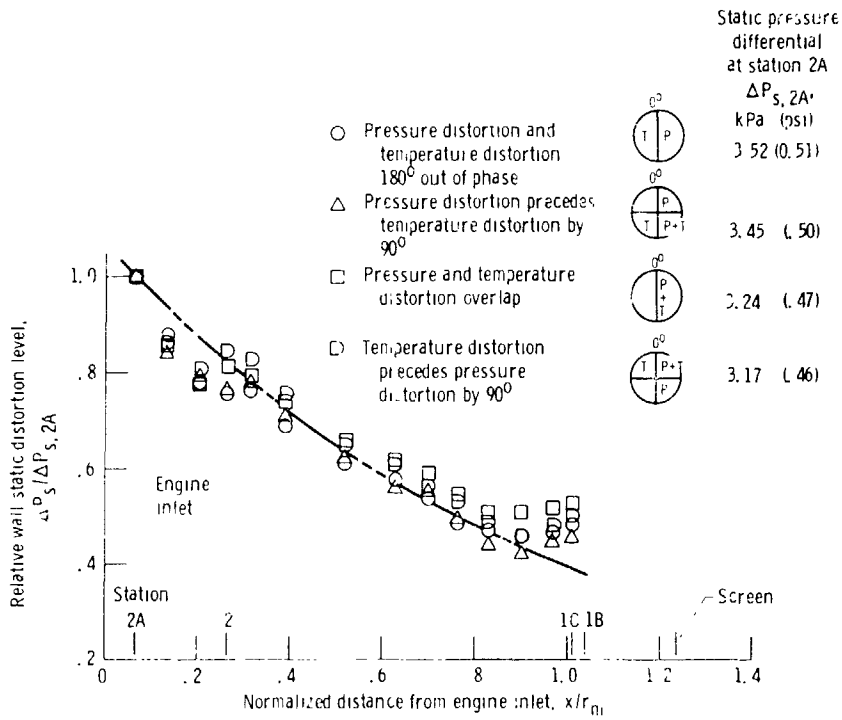

Figure 14. - Effect of total-pressure and total-temperature distortion orientation on static-pressure distortion along inlet-duct wall. See equation (3).

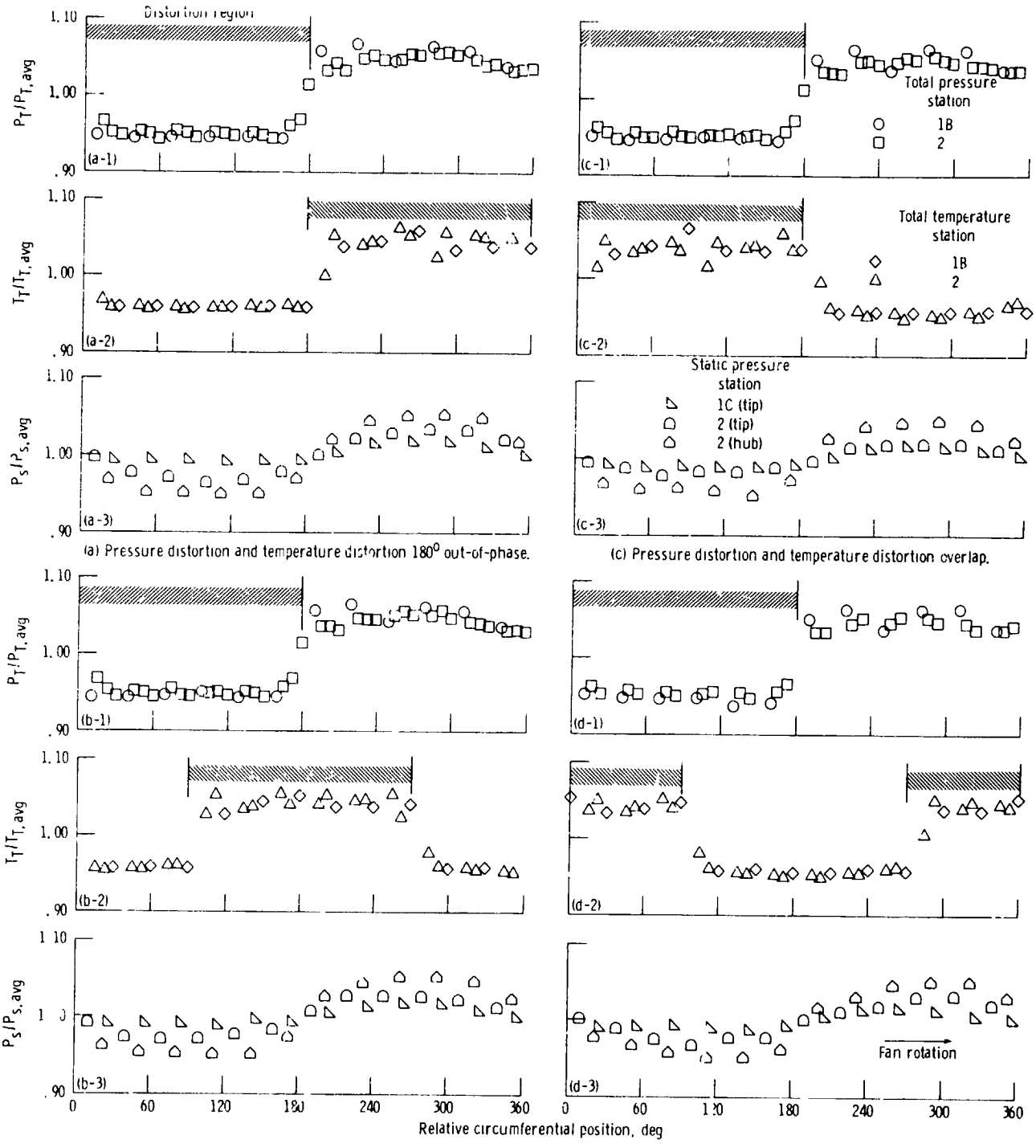

(a) Pressure distortion and temperature distortion 180° out-of-phase.

(b) Pressure distortion precedes temperature distortion by 90°.

(c) Pressure distortion and temperature distortion overlap.

(d) Pressure distortion lags temperature distortion by 90°.

Figure 15. - Circumferential variation of total-pressure, total-temperature and static-pressure profiles along the inlet duct (station 2).

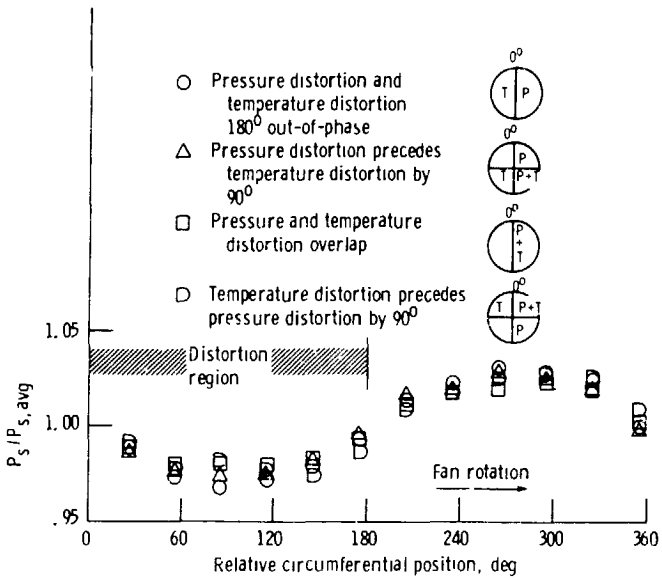

Figure 16. - Circumferential variation of station 2 hub static pressure profiles.

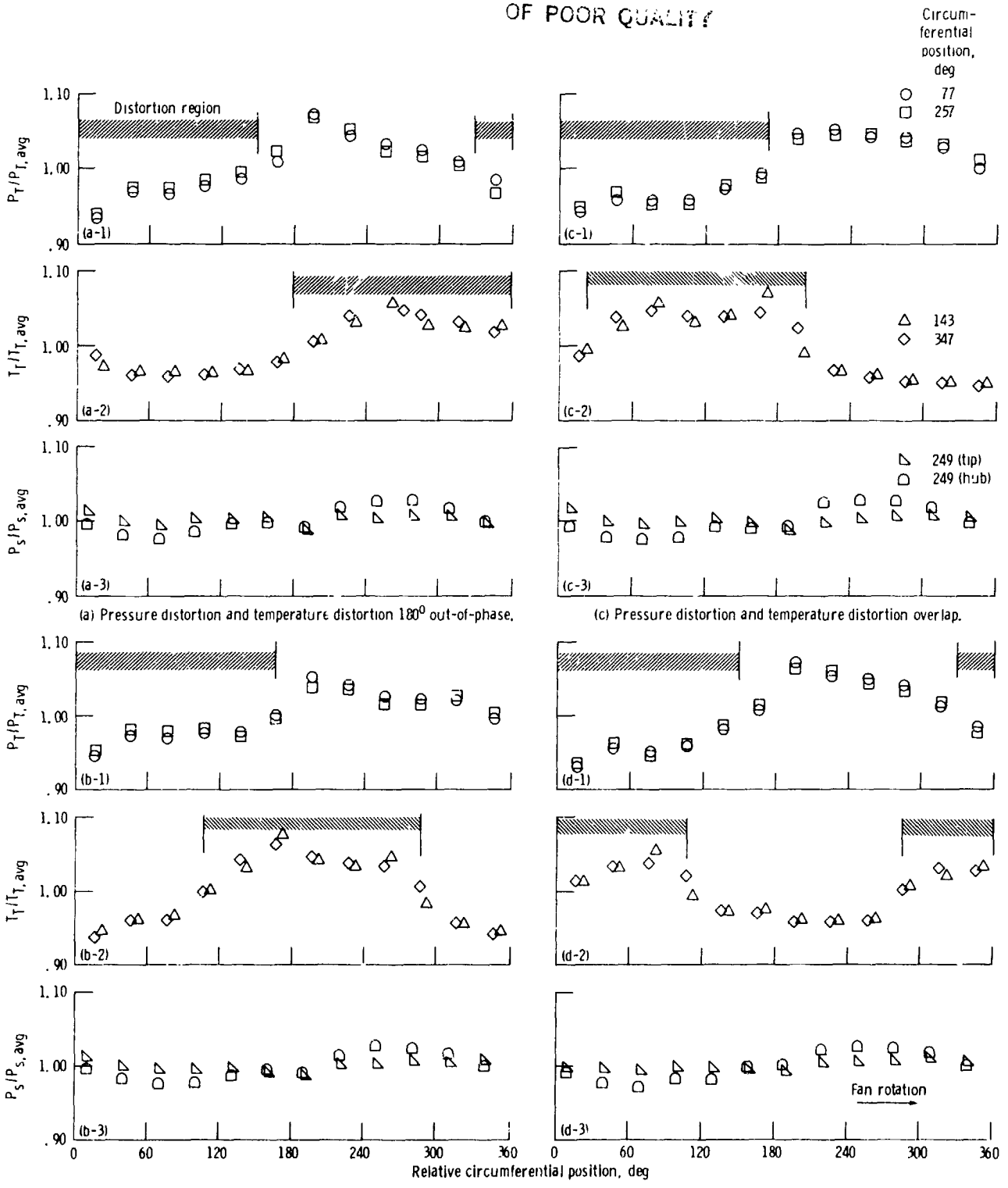

(a) Pressure distortion and temperature distortion 180° out-of-phase.

(c) Pressure distortion and temperature distortion overlap.

(b) Pressure distortion precedes temperature distortion by 90°.

(d) Temperature distortion precedes pressure distortion by 90°.

Figure 17. - Circumferential variation of total-pressure, total-temperature and static pressure profiles at station 2.4.

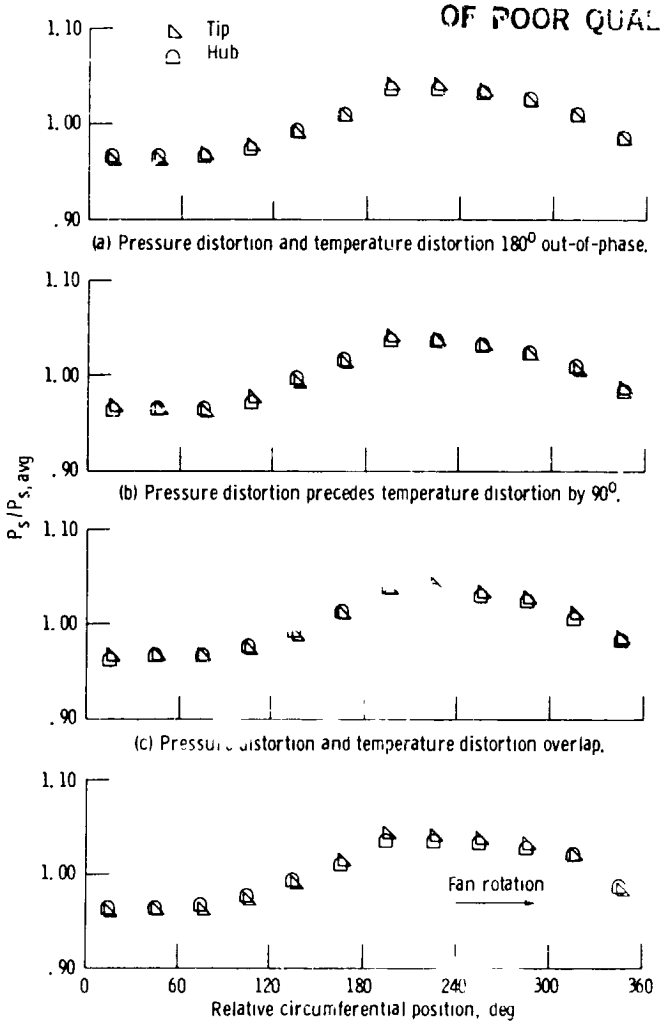

(a) Pressure distortion and temperature distortion 180° out-of-phase.

(b) Pressure distortion precedes temperature distortion by 90°.

(c) Pressure distortion and temperature distortion overlap.

(d) Temperature distortion precedes pressure distortion by 90°.

Figure 18. - Circumferential variation of static pressure profiles at station 2 5. Circumferential position, 225°.

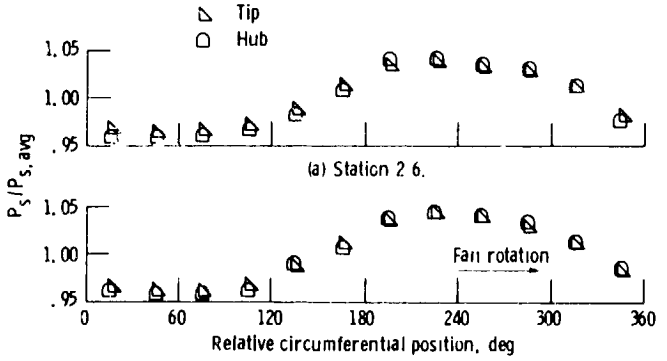

(a) Station 2 6.

(b) Station 2 7.

Figure 19. - Circumferential variation of static pressure profiles at stations 2.6 and 2 7. Circumferential position, 225°.

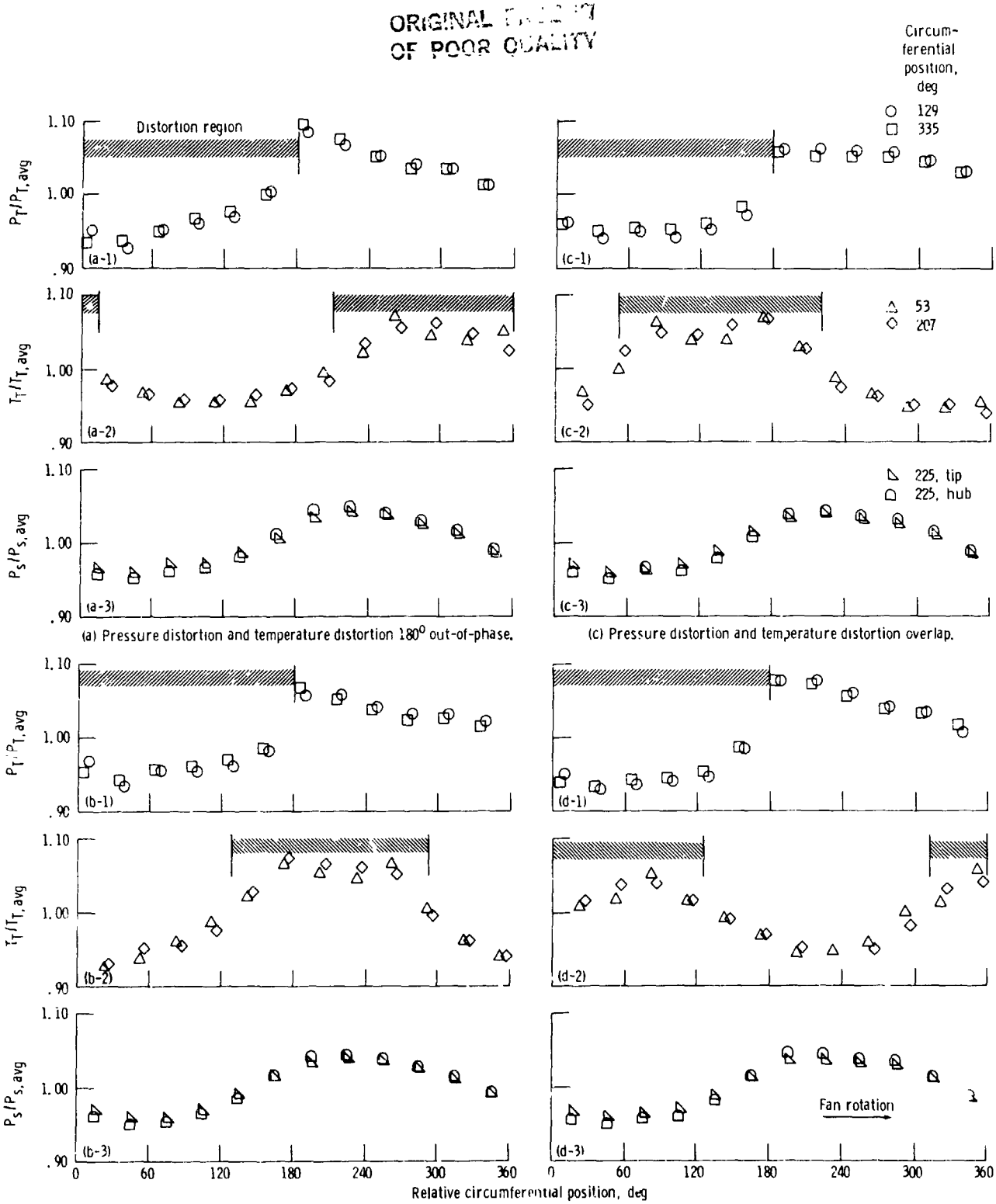

(a) Pressure distortion and temperature distortion 180° out-of-phase.

(c) Pressure distortion and temperature distortion overlap.

(b) Pressure distortion precedes temperature distortion by 90°.

(d) Temperature distortion precedes pressure distortion by 90°.

Figure 20. - Circumferential variation of total-pressure, total temperature, and static-pressure profiles at station 2C.

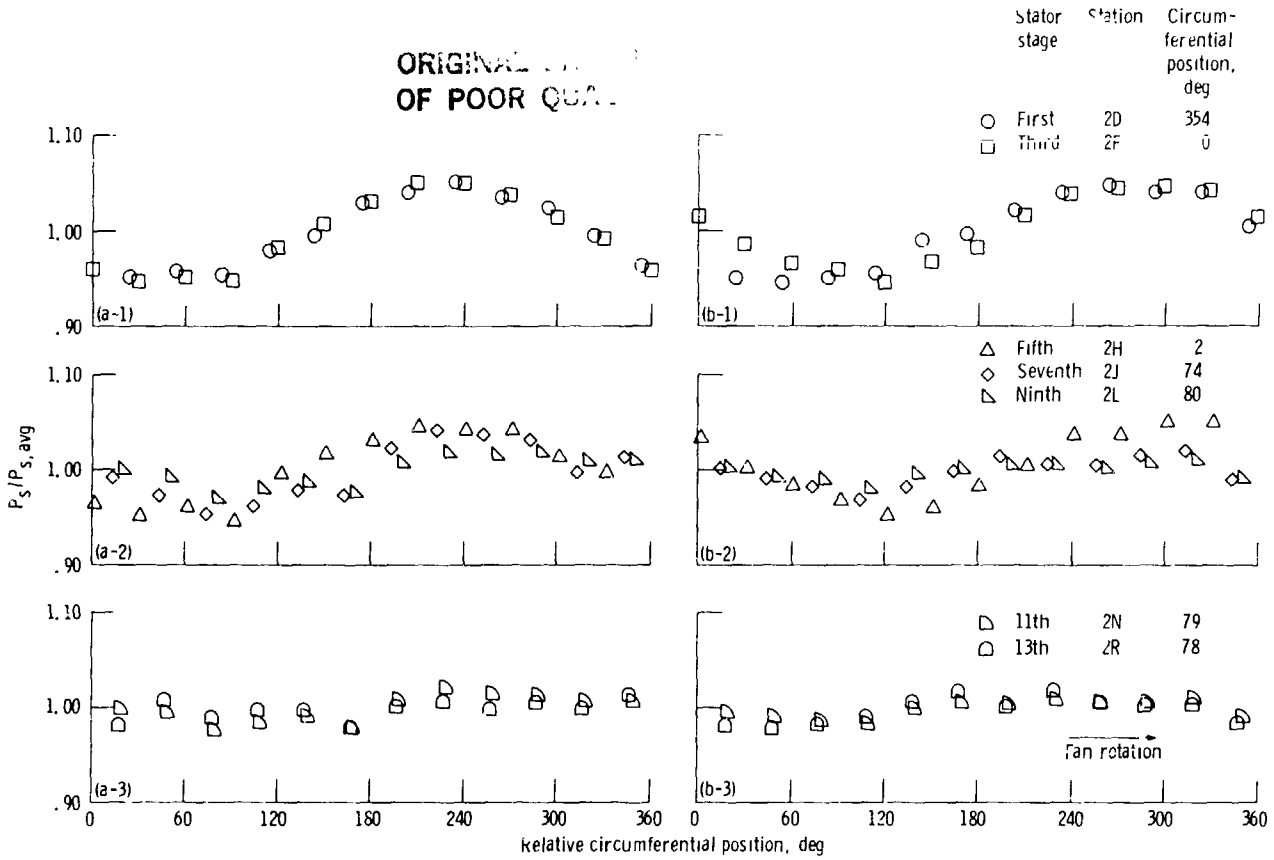

(a) Pressure distortion and temperature distortion are opposed.

(b) Pressure distortion and temperature distortion overlap.

Figure 21. - Circumferential variation of static-pressure profiles at the first stage stators to 13th stage stators inside the compressor (station 2D to station 2R).

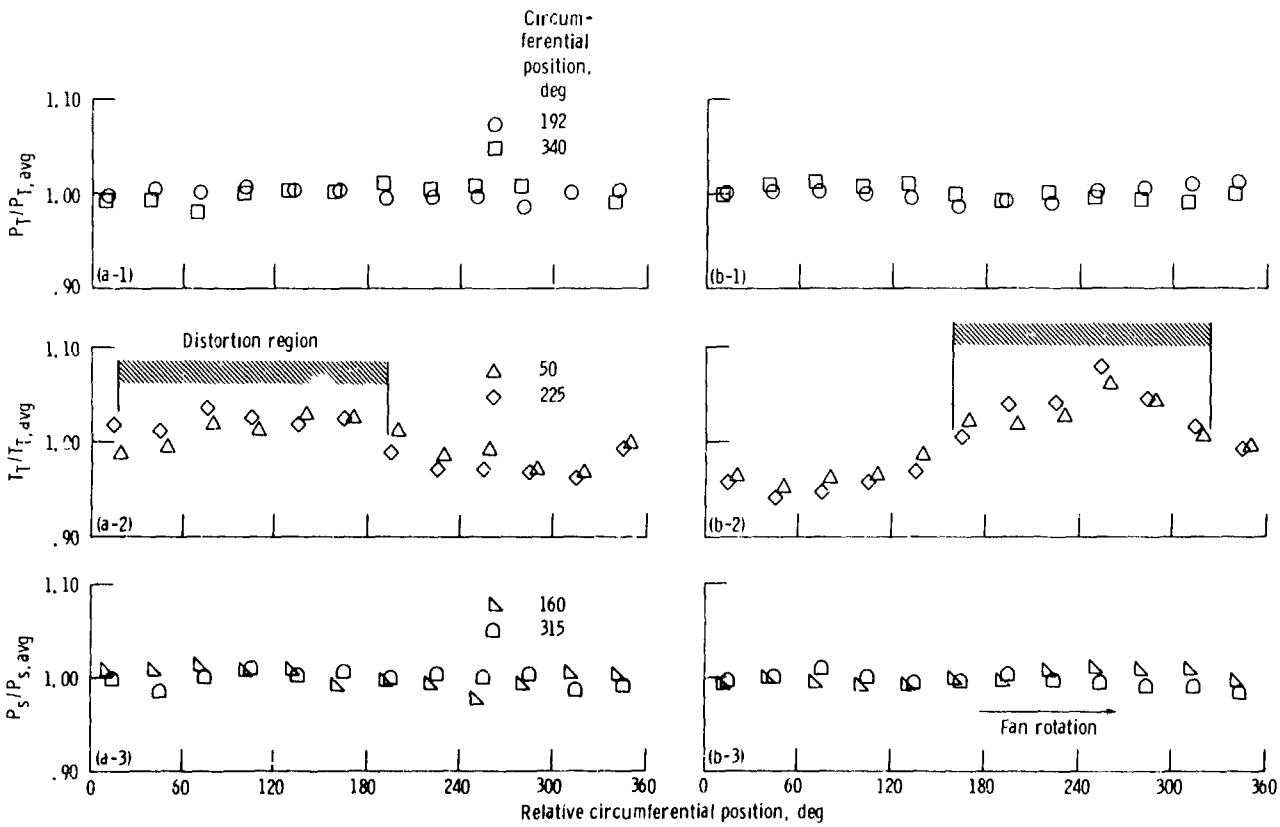

(a) Pressure distortion and temperature distortion 180^0 out-of-phase.

(b) Pressure distortion and temperature distortion overlap.

Figure 22. - Circumferential variation of total-pressure, total-temperature, and static-pressure profiles at station 3.

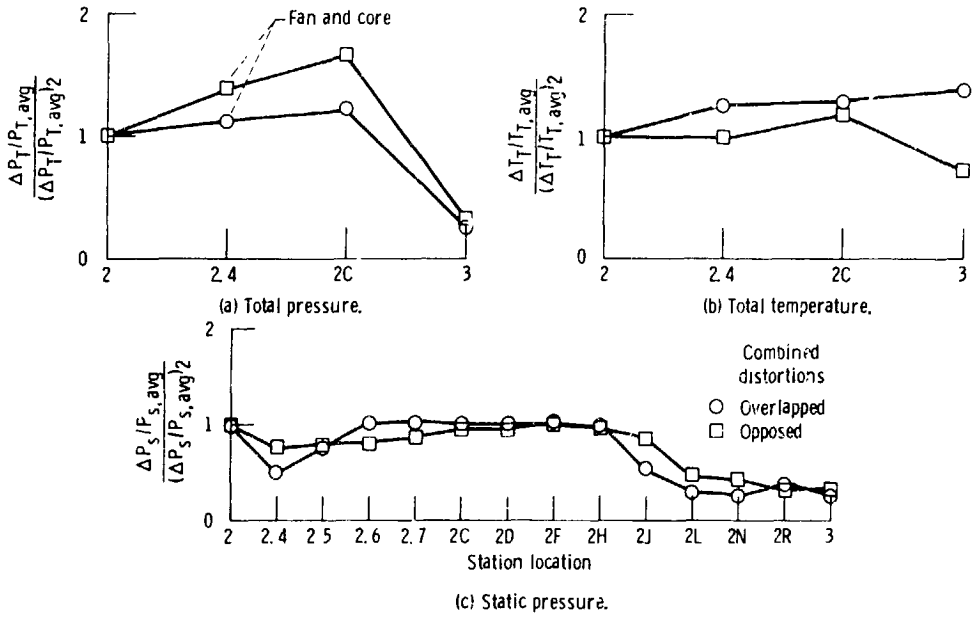

Figure 23. - Effect of distortion orientation on total-pressure, total-temperature, and static-pressure (hub) distortion variation through engine.

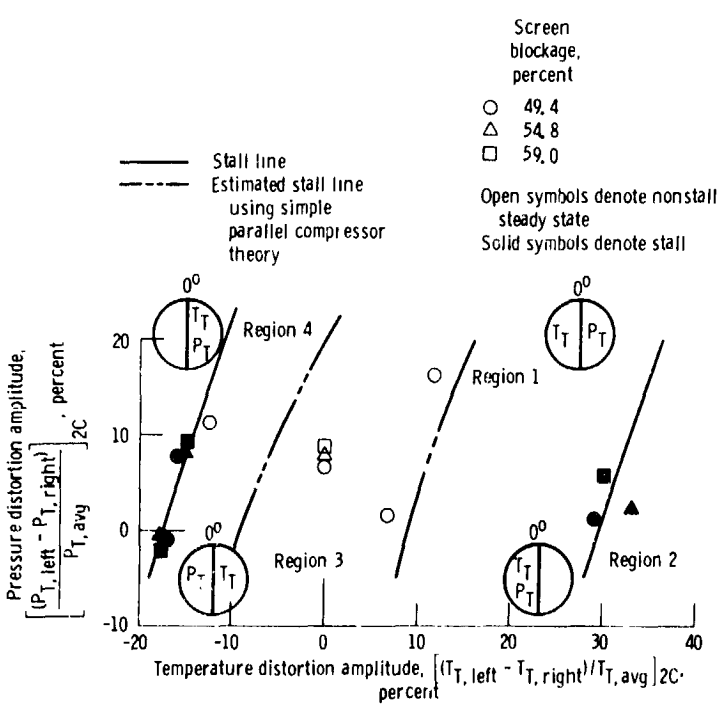

Figure 24. - Distortion sensitivity at compressor inlet (station 2C) for 180°-extent overlapped and opposed total-pressure and total-temperature distortion.